DEPARTMENT OF PHYSICS

ATMOSPHERIC, OCEANIC AND PLANETARY PHYSICS

A Fast Stratospheric Aerosol Microphysical Model (SAMM): H_2SO_4-H_2O Aerosol Development and Validation

S. N. Tripathi
Department of Civil Engineering, Indian Institute of Technology Kanpur, India

X. P. Vancassel, R. G. Grainger
Atmospheric, Oceanic, and Planetary Physics, Clarendon Laboratory, University of Oxford, U.K.

H. L. Rogers
Centre for Atmospheric Science, Department of Chemistry, University of Cambridge, U.K.

AOPP Memorandum 2004.1

27 May 2004

University of Oxford

Abstract

A Fast Stratospheric Aerosol Microphysical Model (SAMM) has been developed to study aerosol behaviour in the lower stratosphere. This model simulates homogeneous binary nucleation, condensational growth, coagulation, and sedimentation of sulphuric acid-water particles in order to predict the composition and size-distribution of stratospheric aerosols. The principal advantage of SAMM is that it is non-iterative, i.e. computing time is reduced by finding semi-implicit solutions to aerosol processes. Condensation and coagulation are solved using the operator-split method. Hence the effect of coagulation is determined in a single iteration. The semi-implicit solution for coagulation agrees well with Smoluchowski's solution for a constant coagulation kernel. Similarly, starting from the fundamental growth equation, a solution for condensational growth is derived that does not require iteration. The solution conserves mass exactly, and is unconditionally stable. In SAMM, homogeneous nucleation and condensation are coupled in a manner that allows realistic competition between the two processes for the limited amount of vapour. With geometrically related size bins (around 40 bins for sulphuric acid-water particles in the range 0.3 nm to 1.5 μm) and an 1800 s time-step, SAMM takes about 3 minutes CPU on a 1.4 GHz computer to calculate the background stratospheric aerosol size distribution. Hence SAMM allows aerosol processes to be included in global models for a relatively small computational expense. SAMM has been used to simulate background stratospheric aerosols and volcanically disturbed aerosol and has been shown to be in good agreement with observations and other modelling studies.

1 Introduction

Stratospheric aerosols can affect the global climate system in a variety of ways. These aerosols play a significant role in the Earth's radiative balance (Lacis et al., 1992) and the attenuation of UV radiation (Michaelangeli et al., 1992). Also, they provide a surface for heterogeneous chemical reactions: these are important for ozone loss in the middle atmosphere (Solomon et al., 1986; Hofmann and Solomon, 1989; Rodriguez et al., 1991). The magnitude of these effects is significantly enhanced when the background aerosol layer is perturbed by strong volcanic eruptions, or possibly by high-speed civil transport aircraft (Tie et al., 1994; Weisentein et al., 1997; Bekki and Pyle, 1992; Pitari et al., 1993).

Stratospheric aerosols are mainly composed of supercooled sulphuric acid droplets (Steele and Hamill, 1981). They may also contain small amounts of other components such as ammonium sulphate (Bigg, 1975; Cadle and Kiang, 1977). The sulphuric acid fraction of the droplets, which is in the range of 50-80 %, is a strong function of the relative humidity and the ambient temperature (Steele and Hamill, 1981), and therefore varies with latitude and season.

Several models have been developed in order to understand the role of stratospheric aerosols in the atmospheric system. A one-dimensional model was developed by Turco et al. (1979) and later refined by Toon et al. (1988) and Zhao et al. (1995). Another class of aerosol microphysical model (0D models) including aircraft plume dynamics has been developed in the last ten years (e.g. Brown et al., 1996; Yu and Turco 1997; Kärcher, 1998). Recently, several studies have been performed where aerosol microphysics has been added to the existing 2D and 3D models. These studies are concerned with the impact of either aircraft emissions (e.g. Bekki and Pyle, 1992; Pitari et al., 1993) or volcanic eruptions (Tie et al., 1994; Bekki and Pyle, 1994; Weistenstein et al., 1997) on the background stratospheric aerosol distribution.

The only 3D study simulating the formation and development of stratospheric aerosols is that reported by Timmreck (2001). In that paper, the emphasis was on the evolution and seasonal variation of stratospheric aerosols using the Hamburg climate model ECHAM4. There is a need for 3D simulations of the effects of aircraft emissions on background stratospheric aerosols, including radiative and chemistry effects. Global studies are important because of the complex interactions between radiation, chemistry and aerosol microphysics. Furthermore, several authors (e.g. Pitari et al., 1993) have pointed out the role of transport when simulating the effects of aircraft sulphur emissions on background stratospheric aerosols.

This paper describes a Stratospheric Aerosol Microphysical Model (SAMM) that is a microphysical box model of sulphuric acid-water aerosols. SAMM has been developed for inclusion in global models. While each of the stratospheric microphysical models described earlier was successful at reproducing the observed background aerosol size distribution parameters, they were all based on iterative methods. Computer processing time and memory use are important issues in global simulations of atmospheric processes: Keeping this in mind, non-iterative solutions to growth and coagulation equations are used in SAMM. These are based on techniques developed by Jacobson (1997, 1999, 2002) and Jacobson and Turco (1995). Jacobson (2002) has successfully applied them to tropospheric aerosols, and this is the first time the techniques have been extended to simulate stratospheric aerosols.

2 Model Description

2.1 Model Overview

The evolution of the size distribution of stratospheric aerosols is described by the continuity equation

$$\frac{\partial N\left(r,t\right)}{\partial t}+\left(\nabla\cdot\left[N\left(r,t\right)\cdot\vec{v}\right]\right)=\left[\frac{dN}{dt}\right]_{\text{micro}}, \tag{1}$$

where N denotes the number concentration of particles in the radius interval r and $r+\Delta r$ at time t, and the second term denotes the advection of particles due to wind motion (v is the wind velocity). The term on the right hand side of the equation is the rate of change of particle number concentration due to microphysical processes, i.e.

$$\left[\frac{dN}{dt}\right]_{\text{micro}}=\left[\frac{dN}{dt}\right]_{\text{nuc}}+\left[\frac{dN}{dt}\right]_{\text{coag}}+\left[\frac{dN}{dt}\right]_{\text{cond}}+\left[\frac{dN}{dt}\right]_{\text{sed}}+\left[\frac{dN}{dt}\right]_{\text{diff}}, \tag{2}$$

where the subscripts nuc, coag, cond, sed, and diff stand for homogeneous nucleation of sulphuric acid-water, coagulation of particles, condensation of sulphuric acid/water onto particles, sedimentation of particles, and diffusion, respectively. Following Turco et al. (1979) and Timmreck and Graf's (2000) assessments of the relative importance of these processes, SAMM includes:

- homogeneous heteromolecular nucleation of H_2SO_4/H_2O,
- condensation and evaporation of H_2SO_4 and H_2O,
- coagulation among the particles,
- sedimentation removal. Figure 1 shows a schematic of the various processes used in SAMM. It can be seen that all the sulphuric acid gas is available for nucleation at the beginning of simulation. Once new particles are formed, they undergo sulphuric acid condensation. As particle growth occurs, all particles are brought to thermodynamic equilibrium with respect to water vapour pressure. Condensation and coagulation are coupled in an operator-split manner. Number concentrations determined from the condensation solution are used to initialise values before coagulation. Finally, larger particles are removed as they undergo a sedimentation process due to gravity effects.

Stratospheric particle distributions usually have radii spanning many orders of magnitude. SAMM has been implemented using N_B geometrically increasing size bins, and the particles have been distributed in these bins as a function of the number of sulphuric acid molecules n_i they contain (Sorokin et al., 2001).

2.2 Condensation of Sulphuric Acid

If the vapour pressure of H_2SO_4 is in excess of the equilibrium vapour pressure then condensation will occur. In the lower stratosphere, where the atmosphere is generally supersaturated with respect to sulphuric acid, condensation occurs, whereas in the upper stratosphere sulphuric acid molecules evaporate from the particles. Jacobson (1997, 1999) gives an equation describing condensational growth of H_2SO_4 onto particles in the size bin i as:

$$\frac{\partial c_{i,t}}{\partial t}=k_{i,t-\Delta t}\left(C_t-S_{i,t-\Delta t}C^{\text{sat}}_{i,t-\Delta t}\right), \tag{3}$$

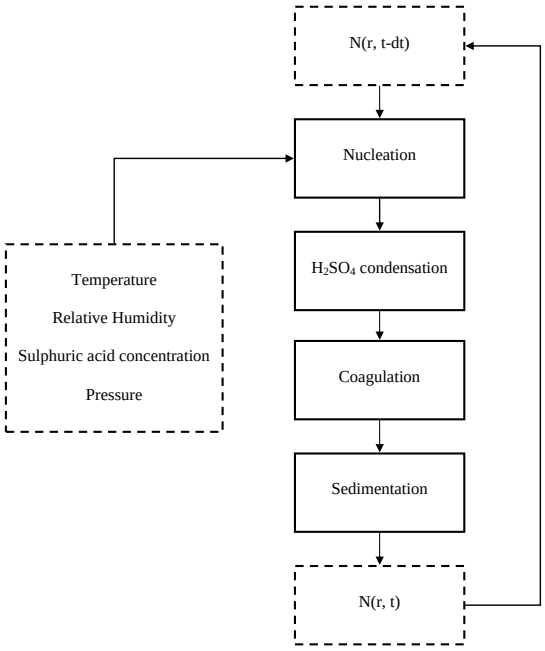

Figure 1: Schematic of the various microphysical processes simulated in the model.

In these and the following equations, the subscripts i, t and $t - \Delta t$ refer respectively to the size bin i considered, the time t and the previous time $t - \Delta t$ at which calculations are carried out. On the left hand side, $c_{i,t}$ is the particle mole concentration of H_2SO_4 (mole m^{-3}). We can also write it as $N_{i,t}n_i/A$, where $N_{i,t}$ is the particle number concentration (m^{-3}) and A is Avogadro's number. On the right hand side of the equation, $k_{i,t-\Delta t}$ is the transfer rate (s^{-1}) between the gas phase and all particles in the bin i. We also use C_t, the ambient H_2SO_4 vapour mole concentration (mole m^{-3}), which is expressed as p/RT, where p is the sulphuric acid vapour pressure (in Pa), R is the universal gas constant (J $mole^{-1}$ K^{-1}) and T is the air temperature in Kelvin. Finally, $C^{\mathrm{sat}}_{i,t-\Delta t}$ is the saturation vapour mole concentration of condensing H_2SO_4 above a flat surface having the same composition as the droplet in bin i (moles m^{-3}). It is also defined as $p^{\mathrm{sat}} \cdot \gamma_i/RT$, where p^{sat} is the saturation vapour pressure above a flat surface of pure sulphuric acid, determined from Ayers et al. (1980) and corrected for low temperatures by Kulmala and Laaksonen (1990), and γ_i is the sulphuric acid activity corresponding to the composition of particles in bin i. The most rigorous method for evaluating the activity coefficient of a solution including ionic solutes has been given by Clegg (1995) and Clegg et al. (1998). However, it is computationally slow and only valid up to a sulphuric acid mole fraction of 0.42. More recently Noppel et al. (2002), have compared the thermodynamic model of Clegg (1995) and Clegg et al. (1998) with the liquid phase activity model of Zeleznik (1991). They found that the resulting sulphuric acid hydrates distribution and nucleation rates, as predicted from the two models, do not differ significantly. Hence we have used the computationally fast activity coefficients given by Zeleznik (1991) in the SAMM. Finally, $S_{i,t-\Delta t}$ is the saturation ratio of sulphuric acid above a curved surface of pure sulphuric acid. This ratio is defined by the Kelvin equation:

$$S_{i,t-\Delta t} = \exp\left(\frac{2\sigma_i V_{\mathrm{m},i}}{r_i RT}\right), \tag{4}$$

where σ_i and r_i are respectively the surface tension (J m^{-2}) and the radius of a particle (m), and $V_{\mathrm{m},i}$ is the volume of sulphuric acid per mole (m^3 mole^{-1}) in a solution having the same composition as a droplet of the considered bin i. The saturation ratio given by Equation 4 takes into account the fact that the saturation vapour pressure above a curved surface is greater than that over a flat surface. There are various other corrections to the saturation ratio because of radiative cooling effects (Jacobson, 1999). However, these are small compared to curvature effects and hence we have not included them at present. Surface tension has been calculated from Vehkamäki et al. (2002) and is written as:

$$\sigma_i(W_i, T) = a(W_i) + Tb(W_i), \tag{5}$$

where W_i is the sulphuric acid weight fraction for a particle in bin i. $a(W_i)$ and $b(W_i)$ are respectively the offset and slope coefficients for the linear dependence of the surface tension on temperature. Condensation of H_2SO_4 molecules onto the droplet surface occurs when the term in brackets on the right hand side of Equation 3 is positive, otherwise H_2SO_4 molecules evaporate from the surface. Equation 3 is a variant of the commonly-used growth equation for stratospheric aerosols that is written as

$$\frac{dr_i}{dt} = \frac{K}{r_i}\left(p - p^{\mathrm{sat}}\right), \tag{6}$$

where K is a prefactor similar but not equal to $k_{i,t-\Delta t}$ (Turco et al., 1979, Weisenstein et al., 1997, Timmreck and Graf, 2000).

To conserve the mass of sulphuric acid between the gas phase and all size bins of the particle phase, the gas-conservation equation must be written as

$$\frac{\partial C_t}{\partial t} = -\sum_{i=1}^{N_B}\left[k_{i,t-\Delta t}\left(C_t - S_{i,t-\Delta t}C^{\mathrm{sat}}_{i,t-\Delta t}\right)\right]. \tag{7}$$

The mass transfer rate used in Equations 7 and 3 can be approximated as

$$k_{i,t-\Delta t} = 4\pi N_{i,t-\Delta t} r_i D_i^{\mathrm{eff}}, \tag{8}$$

where D_i^{eff} is an effective diffusion coefficient (m^2 s^{-1}) taken from Jacobson and Turco (1995) and defined as

$$D_i^{\mathrm{eff}} = \frac{D_i F_i}{1 + \left[\frac{1.33+0.71/Kn_i}{1+1/Kn_i} + \frac{4(1+\alpha_i)}{3\alpha_i}\right] Kn_i}. \tag{9}$$

Here, D_i is the diffusion coefficient of H_2SO_4 molecules (m^2 s^{-1}), Kn_i is the Knudsen number, F_i is the ventilation factor, and α_i is the sticking coefficient of sulphuric acid gas molecules. The expression for D_i is given by (Davis, 1983):

$$D_i = \frac{3}{8Ad^2\rho_{\mathrm{a}}}\left[\frac{RTm_{\mathrm{a}}}{2\pi}\left(\frac{m_{\mathrm{H_2SO_4}} + m_{\mathrm{a}}}{m_{\mathrm{H_2SO_4}}}\right)\right]^{\frac{1}{2}}, \tag{10}$$

where d is the diameter of a sulphuric acid molecule, commonly taken as 4.5×10^{-10} m, $m_{\mathrm{H_2SO_4}}$ is its molecular weight (kg mole^{-1}), m_{a} is the mass of air per mole (kg mole^{-1}) and ρ_{a} is the density of air (kg m^{-3}). The Knudsen number, Kn_i, with respect to particle size r_i, is given by

$$Kn_i = \frac{\lambda}{r_i}, \tag{11}$$

where the mean free path of sulphuric acid gas is given by $\lambda = 3D_i/v_{\mathrm{H_2SO_4}}$ (Fuchs and Sutugin, 1971). Here, $v_{\mathrm{H_2SO_4}}$ is the thermal velocity of H_2SO_4 molecules (m s^{-1}).

The sticking coefficient α_i is an uncertain parameter because no experiments have been conducted under stratospheric conditions. Laboratory experiments under normal conditions (Van Dingenen and Raes, 1991) have quantified a sticking coefficient in the range of $0.028 < \alpha_i < 0.064$ with an average value of 0.04. Clement et al. (1996) from theoretical considerations determined a sticking coefficient $\alpha_i = 1$. We have used this last assumption and made a sensitivity study to see the impact of the choice of such a value (see section 3). To correct the increased rate of vapour and energy transfer to the upstream surface of a large particle ($> 5\mu$m), a ventilation factor for vapour (F_i) needs to be included in the expression for an effective diffusion coefficient. The sizes of particles encountered in stratospheric simulations are small and therefore $F_i = 1$ in this case.

Equations 3 and 7 together represent $N_B + 1$ ordinary differential equations. Most of the microphysical models to date use iterative schemes (such as differential equation solvers) to solve these growth equations. These iterative schemes take considerable computer time. However, our primary concern here is to develop a fast microphysical model that is computationally the least demanding when coupled with large models. We use the non-iterative scheme proposed by Jacobson (1997, 1999) to solve these equations. Assuming that the final concentration can be integrated from equation 7, we get an explicit expression:

$$c_{i,t} = c_{i,t-\Delta t} + \Delta t k_{i,t-\Delta t}\left(C_t - S_{i,t-\Delta t}C^{\mathrm{sat}}_{i,t-\Delta t}\right), \tag{12}$$

where the final H_2SO_4 gas concentration, C_t, is currently unknown. From the mass-balance equation we can write:

$$C_t + \sum_{i=1}^{N_B} c_{i,t} = C_{t-\Delta t} + \sum_{i=1}^{N_B} c_{i,t-\Delta t}. \tag{13}$$

Substituting 12 into 13 and solving for final gas concentration gives

$$C_t = \frac{C_{t-\Delta t} + \Delta t \sum_{i=1}^{N_B} k_{i,t-\Delta t} S_{i,t-\Delta t} C^{\mathrm{sat}}_{i,t-\Delta t}}{1 + \Delta t \sum_{i=1}^{N_B} k_{i,t-\Delta t}}. \tag{14}$$

Substituting Equation 12 into Equation 14 gives

$$c_{i,t} = c_{i,t-\Delta t} + \frac{\Delta t k_{i,t-\Delta t}}{1 + \Delta t \sum_{i=1}^{N_B} k_{i,t-\Delta t}} \times P, \tag{15}$$

where

$$P = C_{t-\Delta t} + \Delta t \sum_{i=1}^{N_B} k_{i,t-\Delta t} S_{i,t-\Delta t} C^{\mathrm{sat}}_{i,t-\Delta t} - S_{i,t-\Delta t} C^{\mathrm{sat}}_{i,t-\Delta t}(1 + \Delta t \sum_{i=1}^{N_B} k_{i,t-\Delta t}) \tag{16}$$

Two limits, however, are used to contain the artificially growing solutions, as suggested by Jacobson (1997). These are

$$C_t = \min(C_t, C) \tag{17}$$

$$c_{i,t} = \max(c_{i,t}, 0) \tag{18}$$

where C is the total sulphuric acid concentration (liquid+gas, in mole m^{-3}). A third limit derived from Jacobson (2002) has been added to the previous ones in order to avoid sulphuric acid evaporation exceeding the total amount of acid included in a particle.

2.3 Condensation of Water

The saturation water vapour pressure $p^{\mathrm{sat}}_{\mathrm{H_2O}}$ over a solution droplet (containing sulphuric acid as solute) is given as (Nair and Vohra, 1975)

$$\ln p^{\mathrm{sat}}_{\mathrm{H_2O}}(W_i) = \frac{2m_{\mathrm{H_2O}}\sigma_i}{RTr_i\rho_i}\left(1 + \frac{W_i}{\rho_i}\frac{d\rho_i}{dW_i} - \frac{3}{2}\frac{W_i}{\rho_i}\frac{d\sigma_i}{dW_i}\right) + \ln p_{\mathrm{H_2O}}, \tag{19}$$

where all the symbols used have already been described except ρ_i which is the density of a particle in the size bin i (kg m^{-3}) determined from Vehkamäki et al. (2002), and $m_{\mathrm{H_2O}}$ (kg mole^{-1}) which is the molecular mass of water. In the case of H_2SO_4, Steele and Hamill (1981) demonstrated that, under stratospheric conditions, the water-vapour pressure over the H_2SO_4-H_2O droplet is equal to the ambient partial pressure of water, i.e. the sulphuric acid weight fraction of a solution droplet is principally a function of water vapour concentration. If environmental conditions change (for example the temperature) so does the water saturation vapour pressure, and this results in a change of sulphuric acid weight fraction and droplet size. However, the solution droplet always remains in equilibrium with respect to atmospheric water vapour (Steele and Hamill, 1981). The rate of collision of water molecules on a stratospheric particle is much higher than that of gaseous sulphuric acid, so particles are assumed to reach water equilibrium instantaneously (found by solving Equation 19).

2.4 Homogeneous Heteromolecular Nucleation

The process of new particle formation (homogeneous nucleation) becomes important only in areas of low temperature and high ambient sulphuric acid concentration (Yue, 1981; Yue and Deepak, 1982). The model uses the homogeneous nucleation theory to describe new particle formation. Although classical theory has never been demonstrated to be accurately able to match observed rates of nucleation, it has been a useful tool to predict trends of new particle formation in the upper tropical troposphere and lower stratosphere (Brock et al., 1995). Indeed, after major volcanic eruptions, such as Mt. Pinatubo, 98% of the observed aerosol is volatile (e.g. Deshler et al., 1992) indicating that homogeneous nucleation is the most important process for stratospheric aerosol formation. Furthermore, the large-scale features of the stratospheric aerosol layer are not very sensitive to the rate of nucleation but are controlled more by coagulation and growth processes (Weisenstein et al., 1997). This justifies our choice of modelling stratospheric aerosols as consisting solely of H_2SO_4-H_2O liquid droplets. Here, we briefly describe the classical nucleation theory. For a more detailed description the reader is referred to, for instance, Kulmala et al. (1998) and Noppel et al. (2002).

The classical nucleation theory describes the formation of a new phase from a mother phase that is becoming unstable. The formation of new particles is assumed to result from the formation of stable clusters that will be able to grow spontaneously after they reach a critical size. This critical size represents, in the case of homomolecular nucleation involving only one condensing vapour, the size or the number of molecules providing the maximum of the Gibbs free energy change, resulting from the phase transition. This maximum is then called the free energy of formation of a particle. In the case of a binary nucleation (here water and sulphuric acid), the Gibbs free energy change is a function of the number of sulphuric acid and water molecules and is represented by a surface. To become stable, a cluster will have to follow the path of least energy on this surface, thus leading to the so-called saddle point (Reiss, 1950). Finding the saddle point using iterative methods is computationally demanding. This is why we used the parameterization of Kulmala et al. (1998), updated

by Vehkamäki et al. (2002). This scheme provides the nucleation rate $J_{\mathrm{H_2SO_4-H_2O}}$ (number of new particles formed per second and per cubic meter) in the water/sulphuric acid mixture, and the critical cluster composition (total number of molecules and sulphuric acid mole fraction). This parameterization is valid at temperatures between 190.15 K and 305.15 K, relative humidities between 0.01% and 100%, and sulphuric acid concentration from 10^4 to 10^{11} cm^{-3}. This range of relative humidity covers the variation found in the global stratospheric relative humidity. These parameterized equations reduce the computing time by a factor of 500 compared to non-parameterized nucleation rate calculations.

Since in the present microphysical model nucleation and growth are coupled, the nucleation rate is first converted to a mass transfer rate between gas and particle, and is then added to the growth mass transfer rate (defined in section 2.2) in the size bin i. More precisely, when $C_{t-\Delta t} > S_{i,t-\Delta t} C^{\mathrm{sat}}_{i,t-\Delta t}$ and $J_{\mathrm{H_2SO_4-H_2O}} > 0$ then the nucleation rate is converted to a gas-phase transfer rate as (Jacobson, 2002)

$$k^{\mathrm{nuc}}_{i,t-\Delta t} = J_{\mathrm{H_2SO_4-H_2O}} \frac{\rho_{\mathrm{H_2SO_4}} V_i f_i}{m_{\mathrm{H_2SO_4}}} \left(\frac{1}{C_{t-\Delta t} - S_{i,t-\Delta t} C^{\mathrm{sat}}_{i,t-\Delta t}} \right), \tag{20}$$

where $\rho_{\mathrm{H_2SO_4}}$ is the density of pure sulphuric acid (kg m^{-3}), V_i is the volume of a single nucleated particle (m^3), and f_i is the volume fraction of sulphuric acid in a nucleated droplet. The mass-transfer rate calculated from equation 20 is then added to the growth mass transfer rate, calculated from equation 8, for the appropriate size bin where all the nucleated particles are placed.

After solving equations 14-18 with the new transfer rates (growth + nucleation), the number concentration of new H_2SO_4-H_2O particles formed due to homogeneous nucleation in the bin i is calculated as

$$N_{i,t} = N_{i,t-\Delta t} + \max(B, 0), \tag{21}$$

where

$$B = (c_{i,t} - c_{i,t-\Delta t}) \frac{m_{\mathrm{H_2SO_4}}}{\rho_{\mathrm{H_2SO_4}} V_i f_i} \frac{k^{\mathrm{nuc}}_{i,t-\Delta t}}{k^{\mathrm{tot}}_{i,t-\Delta t}} \tag{22}$$

and $k^{\mathrm{tot}}_{i,t-\Delta t} = k^{\mathrm{nuc}}_{i,t-\Delta t} + k^{\mathrm{growth}}_{i,t-\Delta t}$.

2.5 Coagulation

Aerosol coagulation is important because it alters the size distribution and the composition of particles, primarily those smaller than one micron in diameter. Since most of the background aerosols found in the stratosphere are of this size, it is necessary to include coagulation within the model. Atmospheric particles collide as a result of Brownian motion, differences in fall velocities, turbulent motion and inter-particle forces. Different approaches have been developed in the past to simulate coagulation, depending upon the need and availability of computer resources. Since the model has to be incorporated into a 3D global chemical transport model, we have concentrated on a semi-implicit scheme which is computationally fast. Aerosol coagulation, in the discrete form, is given by (e.g. Friedlander, 2000)

$$\frac{\partial N_{k,t}}{\partial t} = \frac{1}{2} \sum_{j=1}^{k-1} K_{j,k-j} N_{k-j,t} N_{j,t} - N_{k,t} \sum_{j=1}^{\infty} K_{k,j} N_{j,t}, \tag{23}$$

where $K_{k,j}$ is the coagulation kernel of two colliding particles (m^3 s^{-1}). Using semi implicit finite differencing, we obtain a general formula for a volume-conserving solution of uniform composition

(Jacobson et al., 1994)

$$V_k N_{k,t} = \frac{V_k N_{k,t-\Delta t} + \Delta t \sum_{j=1}^{k} \left(\sum_{i=1}^{k-1} \theta_{i,j,k} K_{i,j} V_i N_{i,t} N_{j,t-\Delta t} \right)}{1 + \Delta t \sum_{j=1}^{N_B} \left(1 - \theta_{k,j,k}\right) K_{k,j} N_{j,t-\Delta t}}, \tag{24}$$

where V_k is the volume of the k-monomer particle. In equation 24 it can be seen that no production occurs in the first bin, $k = 1$, since $k - 1 = 0$. Thus all $N_{i,t}$ terms are known while calculating $N_{k,t}$. The intermediate particles between two bins are partitioned using $\theta_{i,j,k}$, given by Jacobson et al. (1994) as

$$\theta_{i,j,k} = \begin{cases} \left(\frac{V_{k+1} - V_{i,j}}{V_{k+1} - V_k}\right) \frac{V_k}{V_{i,j}} & ; V_k < V_{i,j} < V_{k+1} \quad ; k < N_B \\ 1 - \theta_{i,j,k-1} & ; V_{k-1} < V_{i,j} < V_k \quad ; k > 1 \\ 1 & ; V_{i,j} \geq V_k \quad ; k = N_B \\ 0 & \text{other} \end{cases} \tag{25}$$

where $V_{i,j} = V_i + V_j$. The generalised Brownian coagulation kernel, $K_{i,j}$, is taken from Fuchs' (1964) interpolation formula

$$K_{i,j} = \frac{4\pi(r_i + r_j)(D_i^{\mathrm{p}} + D_j^{\mathrm{p}})}{\frac{r_i + r_j}{r_i + r_j + (\delta_i^2 + \delta_j^2)^{1/2}} + \frac{4(D_i^{\mathrm{p}} + D_j^{\mathrm{p}})}{(r_i + r_j)((V_i^{\mathrm{p}})^2 + (V_j^{\mathrm{p}})^2)^{1/2}}}, \tag{26}$$

where the particle diffusion coefficient D_i^{p} is given by

$$D_i^{\mathrm{p}} = \frac{k_B T C_c}{6\pi r_i \eta_{\mathrm{a}}}, \tag{27}$$

where the Cunningham-slip factor, C_c, is defined as

$$C_c = 1 + Kn_i \left(1.249 + 0.42\mathrm{e}^{-0.87/\mathrm{Kn_i}}\right). \tag{28}$$

The Knudsen number $Kn_i = \lambda_{\mathrm{a}}/r_i$ is determined from the mean free path of air molecules, λ_{a}, which is given by

$$\lambda_{\mathrm{a}} = 2\eta_{\mathrm{a}}/\rho_{\mathrm{a}} v_{\mathrm{a}}, \tag{29}$$

where η_{a} is the dynamic air viscosity (kg m^{-1} s^{-1}) calculated from List (1984):

$$\eta_{\mathrm{a}} \approx 1.83 \times 10^{-7} \left(\frac{416.16}{T + 120}\right) \left(\frac{T}{296.16}\right)^{\frac{3}{2}}; \tag{30}$$

ρ_{a} is the air density and v_{a} is the thermal velocity of air molecules (m s^{-1}) calculated from

$$v_{\mathrm{a}} = \sqrt{8 k_{\mathrm{B}} T / \pi m_{\mathrm{a}}} \tag{31}$$

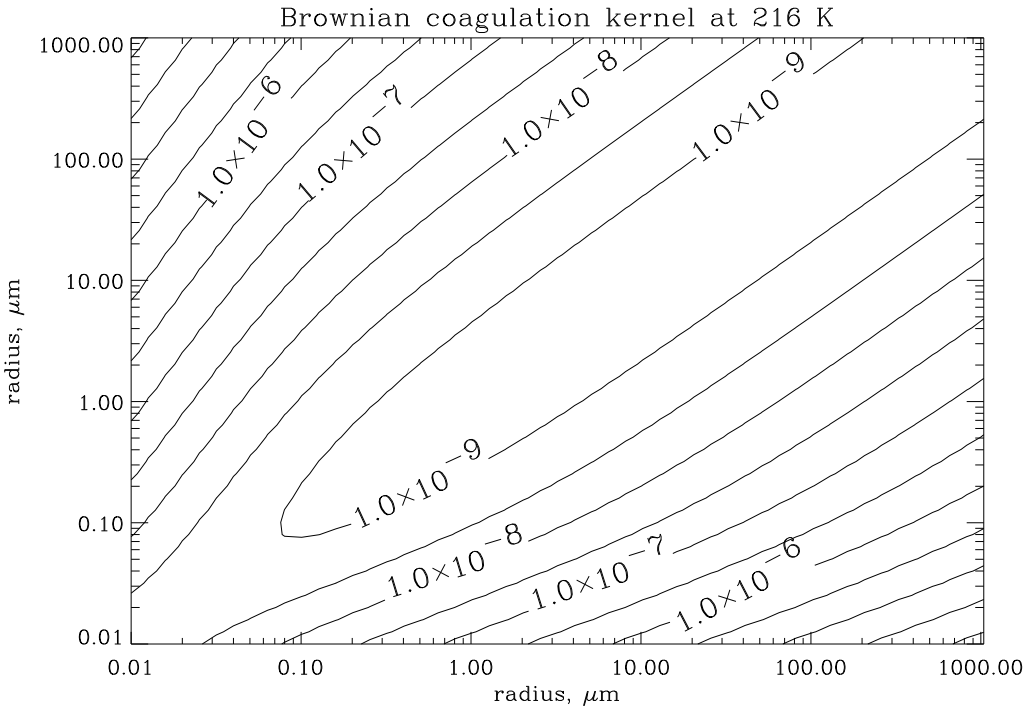

Figure 2: Brownian coagulation kernel ($\mathrm{cm}^3\ \mathrm{s}^{-1}$) plotted as a function of particle radius at 216 K.

where k_B is the Boltzmann constant. The mean distance from the centre of a sphere reached by a particle leaving the surface of the sphere and travelling a distance of particle mean free path, δ_i, is found from

$$\delta_i = \frac{(2r_i + \lambda_i^\mathrm{p})^3 - (4r_i^2 + (\lambda_i^\mathrm{p})^2)^{3/2}}{6r_i\lambda_i^\mathrm{p}} - 2r_i, \tag{32}$$

where the particle mean free path λ_i^p is defined

$$\lambda_i^\mathrm{p} = \frac{8D_i^\mathrm{p}}{\pi v_i^\mathrm{p}}, \tag{33}$$

where v_i^p is the particle thermal velocity ($\mathrm{m\ s}^{-1}$) . Other coagulation kernels (gravitational collection, turbulent inertial motion and turbulent shear motions) are not included because they are much smaller compared to the Brownian kernel in typical stratospheric conditions.

The coagulation equations for particles of different composition (for example water-sulphuric acid) can be written in a similar manner to Equation 24:

$$V_k N_{k,t} = \frac{V_k N_{k,t-\Delta t} + \Delta t \sum_{j=1}^{k} \left(\sum_{i=1}^{k-1} \theta_{i,j,k} K_{i,j} V_i N_{i,t} N_{j,t-\Delta t} \right)}{1 + \Delta t \sum_{j=1}^{N_B} \left(1 - \theta_{k,j,k}\right) K_{k,j} N_{j,t-\Delta t}}. \tag{34}$$

Brownian coagulation kernels obtained from equation 26 at 216 K are plotted in figure 2. From this plot, it is clear that the smallest value of the kernels occurs when both particles are of the same size. The coagulation kernel rises rapidly when the ratio of the particles radii diverges from unity. This increase is due to the interplay between size and velocity of two colliding particles. A large particle has a small velocity but it provides a large surface area compared to a very fast small particle, thus the result is a large coagulation rate. In the event of two small particles colliding, the coagulation kernel is small because of their small cross-sectional area.

2.6 Sedimentation

The sedimentation mechanism is responsible for the descent of particles from one layer to another and thus it affects the size distribution of stratospheric particles under the influence of gravity. Assuming that all the particles are spherical, sedimentation velocity, $v_i^{\rm sed}$, is given as (Pruppacher and Klett, 1997)

$$v_i^{\rm sed} = \frac{2(\rho_i - \rho_{\rm a}) C_c r_i^2 g}{9\eta_{\rm a}}, \tag{35}$$

where g is the gravitational constant in m s^{-2}.

3 Selection of Model Parameters

Computer processing memory is an important issue in global simulations. The present microphysical model is intended to be included in a 3D global chemical model (SLIMCAT) to simulate the effects of aircraft emissions on background aerosols. Keeping this in mind, we have performed several sensitivity studies in order to see the effects of the choice of the number of size bins used on the predicted aerosol size distribution features. The upper and lower size limits adopted for SAMM are roughly 1.5 μm and 0.3 nm respectively. This upper size limit is based on the fact that in typical stratospheric conditions very few water-sulphuric acid particles become larger than this size, and those that do rapidly sediment. The lower size limit is set by the size of the newly formed particles estimated from classical nucleation theory. When using a larger number of size bins, the aerosol distribution is better resolved. But the integration time step is also a very important parameter. The smaller the time step, the more accurate the results that are expected. We performed a benchmark calculation using roughly 300 size bins (against 44, for example, in Timmreck and Graph's runs, 2000) and a relatively small time step of integration (600 s, which is 3 times smaller than typical dynamical time steps used in 3D models). Such a calculation provides accurate results but is computationally slow and demanding. In order to find the best compromise between accuracy and computing time required, we performed a sensitivity study: this was done by changing the number of bins and time steps. Results (surface area density, particle number concentration, volume density) have then been compared to our reference case, the benchmark run. Figure 3 (top) plots the background aerosol surface area density (SAD, surface per unit volume of air) as a function of the number of size bins and the integration time-step for conditions typical of an altitude of 20 km. The calculated SAD lie between 0.5×10^{-9} and 6.5×10^{-9} cm^2 cm^{-3} (0.5 and 0.65 μm^2 cm^{-3}). These values are comparable to those recommended for heterogeneous chemical reactions of atmospheric importance. Tie et al. (1994) reported a value of 0.6 μm^2 cm^{-3} for aerosol SAD at 20 km from their 2D model calculations. It can be seen that little accuracy is gained by decreasing the model time step below about 2000 s.

Therefore all the standard model runs used an 1800 s time-step which is indicated on the figure (dashed line). It can also be seen that the number of size bins does not have a pronounced effect on the calculated aerosol SAD, since the model results differ by only 25% using 10 or 300 bins. Figure 3 (bottom panel) plots the variation of particle surface density with number of size bins for an 1800 s time-step. The surface area density reaches its asymptotic value when the number of bins chosen is greater than ≈ 100. From this plot, we can estimate the difference of aerosol SAD between the 40 bins case and the benchmark (300 bins) to be around 5%.

Figure 4 shows the effects of number of size bins and integration time-step on three moments of particle size distribution.

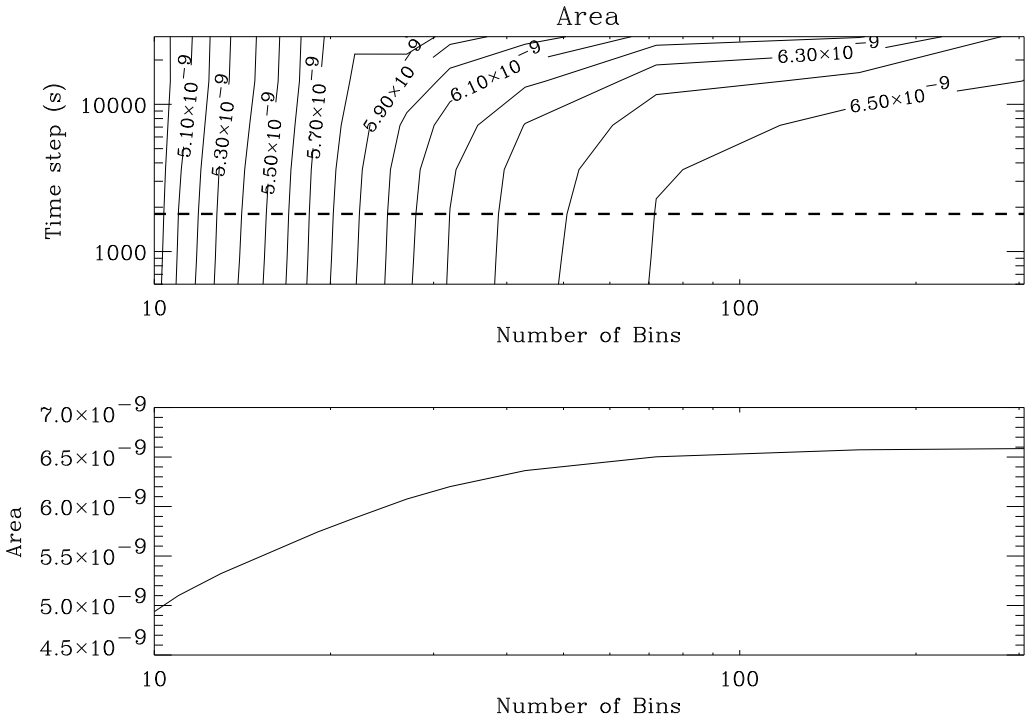

Figure 3: Top: Aerosol surface area density (m^2 m^{-3}) plotted as a function of the number of size bins used and the integration time-step. Bottom: Aerosol surface area density vs number of size bins for an integration time-step of 1800 s. Initial parameters adopted are: temperature = 216 K, water vapour pressure = 3.68 mb, sulphuric acid concentration = 0.048 μg m^{-3}.

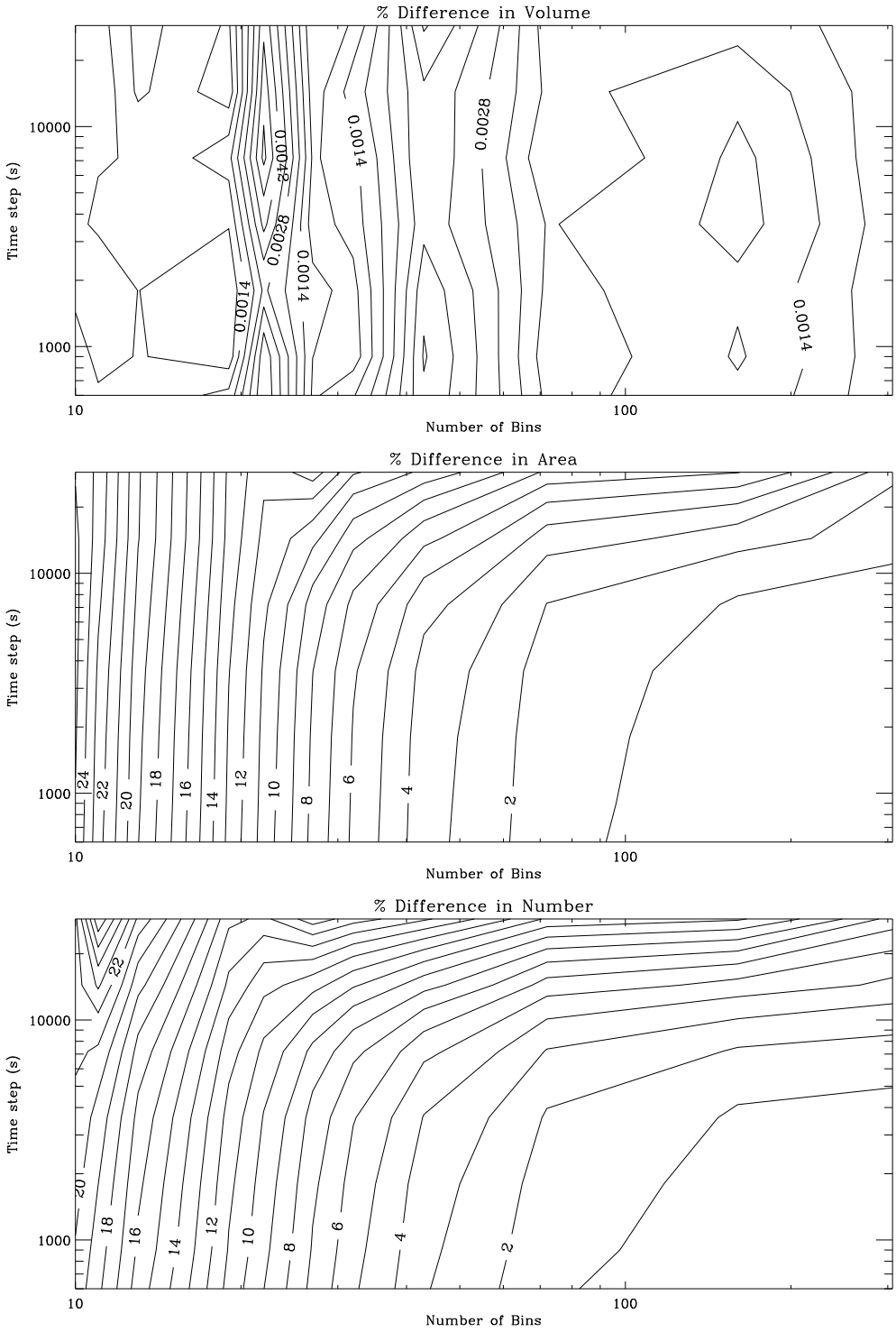

Figure 4: Top: Percentage difference in total particle volume density relative to benchmark value. The benchmark value is the best estimate of particle distribution using 306 size bins and 600 s integration time step. Middle: Same as the plot at the top except for aerosol surface area density. Bottom: Same as the top one except for number concentration.

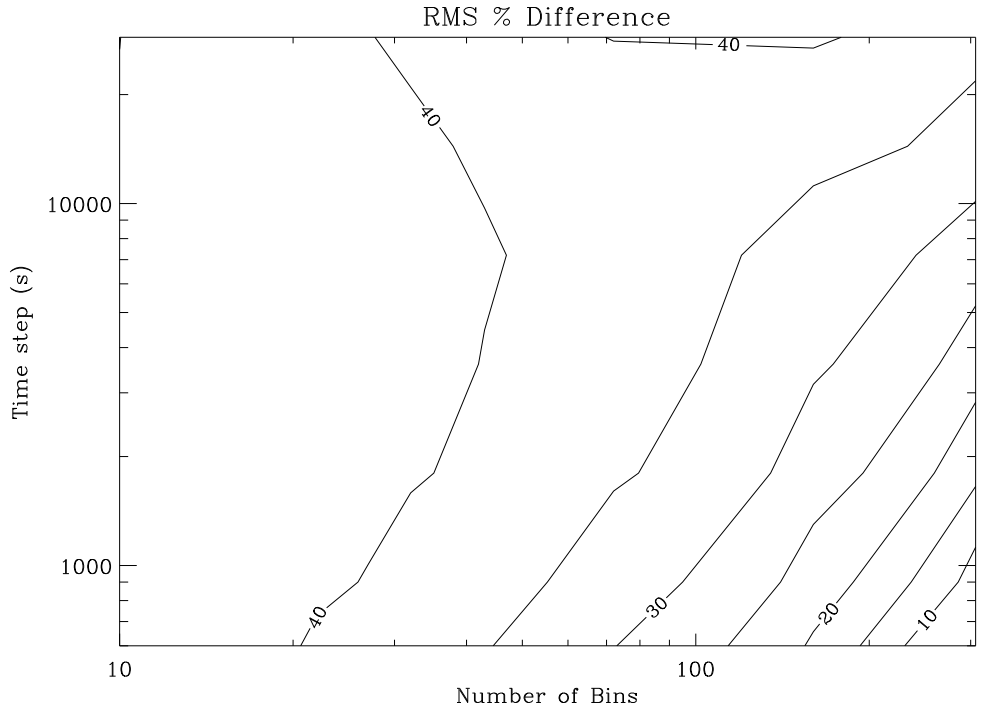

Figure 5: Root mean square error as a function of number of size bins and integration time-step for a size distribution relative to the benchmark size distribution.

In figure 4 (top) we plot the percentage difference from the benchmark run of the total particle volume density obtained using different numbers of bins and integration time-steps.

First, the percentage difference doesn't depend on the number of bins or the time step used, as we find the same value using 20 or 200 bins at the same time step (e.g. 0.0014 around 2000 s). The second point is that the percentage difference is very small (less than 0.5%) and shows how accurate the numerical scheme is as it conserves volume. These observations indicate that the difference observed between the benchmark run and other calculations is not significant. Figure 4 (middle panel), shows the percentage difference (from the benchmark) of the aerosol SAD as a function of the number of size bins and the integration time-step used. The percentage difference in surface area density increases as the number of bins decreases, which is as expected, but remains fairly small (maximum of $\approx 25\%$ of difference). Figure 4 (bottom panel) shows the percentage difference in particle number concentration (0^{th} moment) plotted as a function of number of size bins and integration time-step. We see that percentage difference increases as number of size bins decreases. This clearly indicates that using coarse resolution bins results in only a small error when calculating total number concentrations, surface and volume densities. Our main concern remains the ability to get an accurate value for the SAD, as heterogeneous chemistry strongly depends on it. Hence, these tests are satisfactory but we have to keep in mind that the tail of the aerosol size distribution could be artificially broadened when using a small number of bins.

Figure 5 shows this result more explicitly, giving the ($\%$) root mean square (rms) difference between the calculated size distribution at 20 km and the benchmark distribution. For an 1800 s time step, the % rms difference is as high as 40 % when the number of bins is about 40.

A sensitivity study was also performed to see the effect of the H_2SO_4 molecules' sticking coeffi-

cient (α_i) on the modelled size distribution. Changing α_i from 0.01 to 1 did not make a significant difference to the modelled size distribution. Hence, we use a fixed value of 1 for α_i in SAMM. The same value has been used to describe the sticking coefficient between colliding particles (i.e. their collision efficiency), as sulphuric acid-water particles are likely to attach very efficiently.

A time step of 1800 s and a bin number of approximately 40 (depending on the geometrical increase used) was adopted for SAMM. Based on this evaluation, we expect computational errors $<$ 0.005 %, 5 % and 40 % in the volume, surface area and number densities respectively.

4 Validation

The coagulation scheme and its efficiency as a function of the number of size bins used have been investigated. Figure 6 compares the semi-implicit solution after 12 hours of simulation to the Smoluchowski's analytical solution given by

$$N_{k,t+1} = \frac{N_t(0.5N_tK_{i,j}\Delta t)^{k-1}}{(1+0.5N_tK_{i,j}\Delta t)^{k+1}}, \tag{36}$$

where the constant coagulation kernel $K_{i,j} = 8k_BT/3\eta_{\mathrm{a}}$.

Figure 6 shows that the solution from the semi-implicit numerical approach matches very closely the analytical solution when the number of bins used is large. It confirms also that the tail of the size distribution is dramatically modified when using a small number of bins.

Figure 7 (top) shows the evolution of particles' size spectra for coagulation alone, using a time step of 600 s. Figure 7 (bottom) plots the evolution of particle size distribution due to all processes happening together. Comparing figures 7 top and bottom, one can note that due to growth, particles are becoming larger and the size spectrum is shifting more towards the larger particles. It can also be seen that large particles are removed and the size distribution shifts towards smaller sizes when sedimentation is included. An important finding is that results appeared to be very sensitive to the sedimentation scheme used. In particular, when using a single box model, when mass has to be conserved, the question of replacement of the sulphuric acid lost by sedimentation is important. Replacing it by gaseous sulphuric acid can lead to a burst of nucleation (Timmreck and Graf, 2000). In reality, the loss of mass by sedimentation is balanced by falling particles from upper layers and also by advection or even convection. In the present study, transport phenomena have been neglected. Hence, all the sulphuric acid lost by sedimentation has been replaced by the same mass in the gas phase.

We have performed a number of validation studies with this model and compared the calculated size-distribution parameters with some observed values, an analytical solution and a benchmark run. These studies are important at this point and have served to test the ability of the model to reproduce the parameters of stratospheric aerosols before coupling it to global models.

Several measurements of stratospheric aerosol size distribution exist, from in situ (optical particle counter) to remote sensing (e.g. satellite, lidar). To retrieve particle size distribution, remote sensing techniques rely on additional information from theoretical models; hence we chose to compare the modelled aerosol population parameters with only in situ observations and previous modelling studies.

Since the early seventies, a continuous time series of regularly flown vertical balloon profiles is available for Laramie, Wyoming (41°N) (Hofmann et al., 1975; Hofmann and Rosen, 1981; Deshler

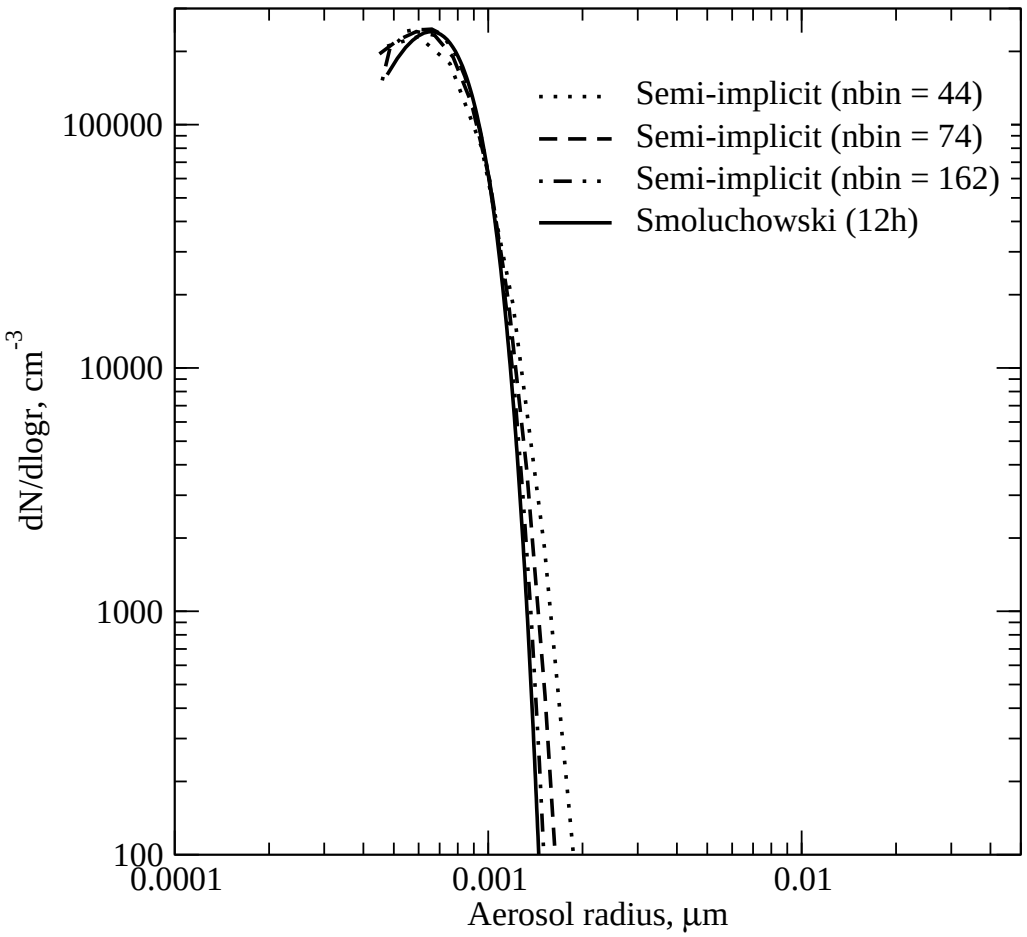

Figure 6: Comparison of semi-implicit results with Smoluchowski's analytical solution for different numbers of size bins.

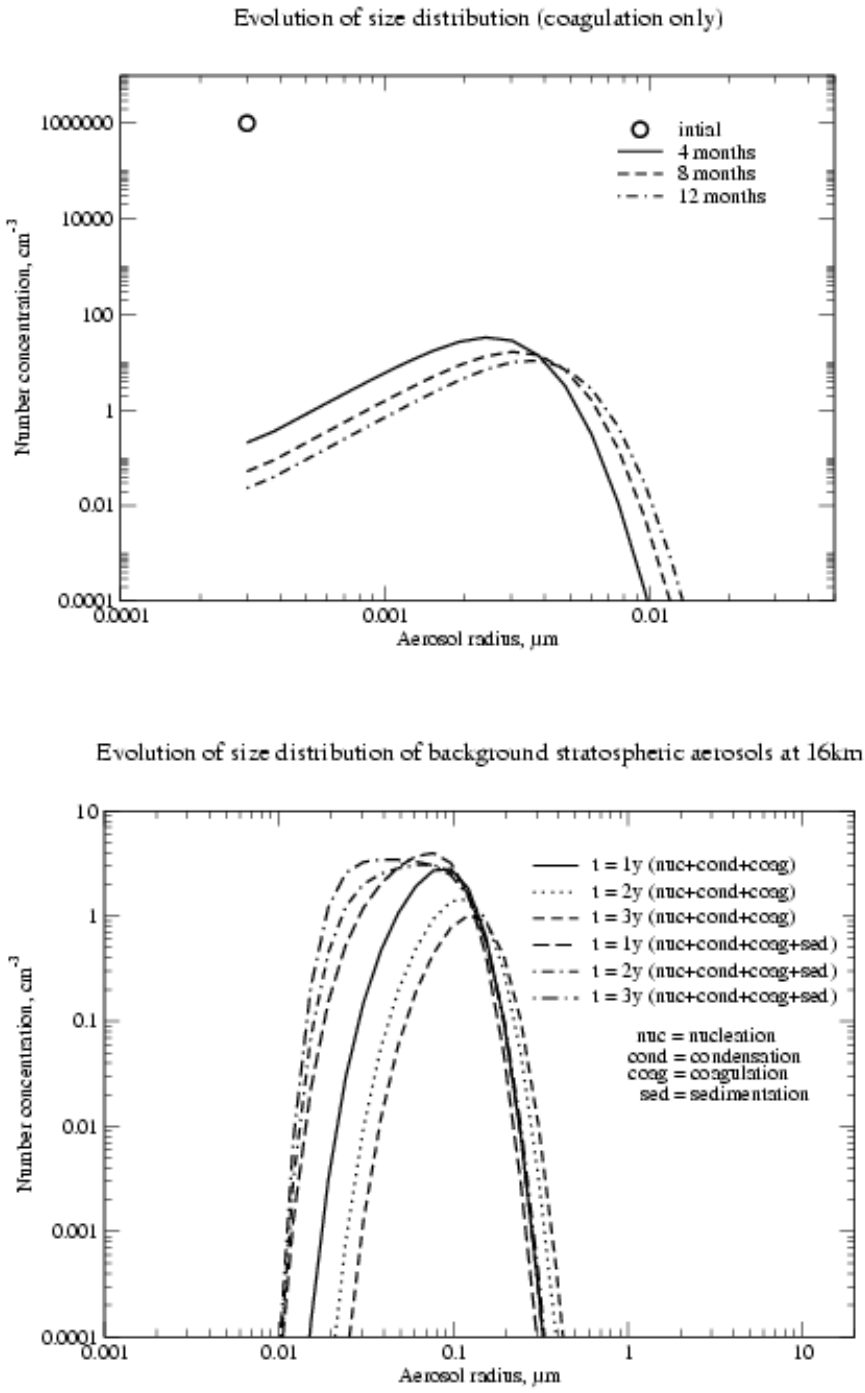

Figure 7: Top: Evolution of particle size distribution undergoing Brownian coagulation only at different times. Bottom panel: Evolution of nucleated particle size distribution by condensational growth, coagulation and sedimentation at different simulation times, 1 year, 2 years and 3 years (1y, 2y, 3y).

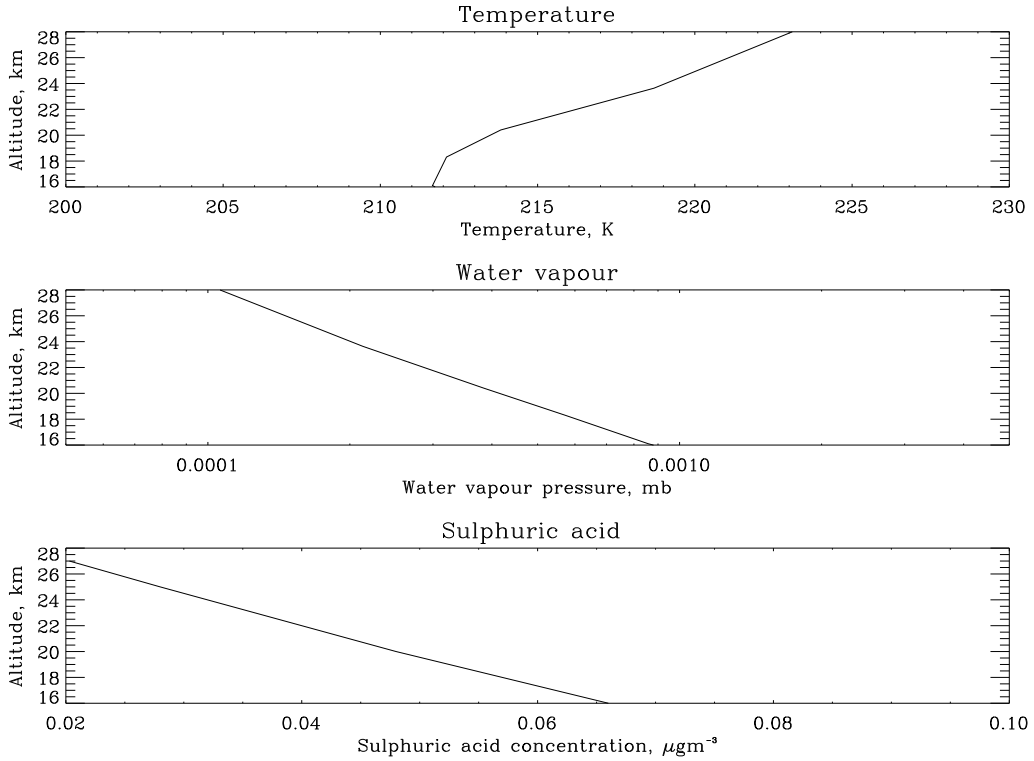

Figure 8: Top: Zonally averaged temperature profile for Laramie, Wyoming taken from ECMWF reanalysis data. Middle: Same as the top panel except for water vapour pressure. Bottom: Sulphuric acid concentration profile as taken from Toon et al. (1979).

et al., 1992; Deshler et al., 1993). These are based on optical particle counting techniques and give vertical profiles of particle mixing ratios (number of particles whose radius is larger than 0.15 μm and 0.25 μm per mg of air). Also, a number of observational profiles are available for the Arctic and the Antarctic (Hofmann and Solomon, 1989; Hofmann et al., 1992) and from global observations of aerosol size distribution (e.g. Rosen et al., 1975).

In the following experiments, we used zonally averaged temperature and relative humidity profiles from ECMWF reanalysis data for Laramie, Wyoming as given in figure 8, top and middle panel respectively, where most of the stratospheric aerosol observations are being carried out. There is no consensus as such with respect to the sulphuric acid gaseous concentration in the stratosphere, most of which is found in particle phase. There are several ways to initialise the model for sulphuric acid gaseous concentration: for example by coupling the aerosol model and a chemical model with sulphur chemistry. However, at each altitude we used the sulphate concentration data from Toon et al. (1979), plotted in figure 8 (bottom).

The figure 9 plots show the evolution of the aerosol features with altitude. The surface area and the volume densities decrease with altitude as temperature rises and sulphuric acid concentration decreases. Under such conditions, nucleation is then less efficient at producing new particles, and the calculated profiles obtained as a function of altitude were as expected.

In figure 10 we plot model-simulated aerosol mixing ratios (N15, number of particles larger than 0.15 μm per mass of air) together with observed values from Hofmann and Rosen (1981) and previous model results (note that for particles larger than 0.25 μm, the mixing ratio is N25). Whatever

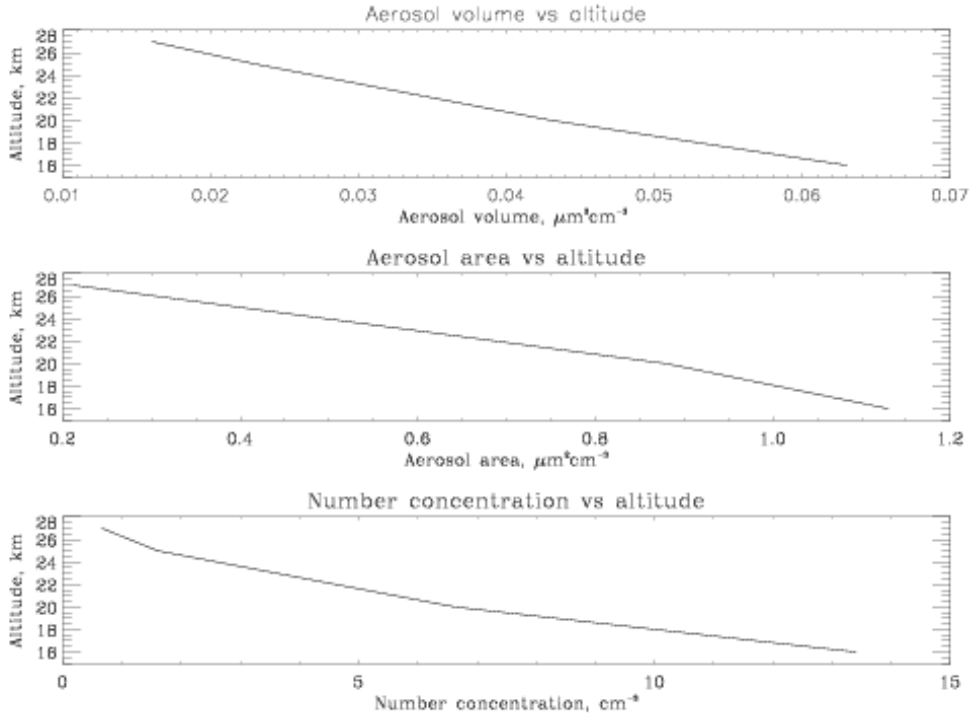

Figure 9: Top: Aerosol volume density vs altitude for Laramie, Wyoming. Middle: Same as top except for aerosol surface area density. Bottom: Same as top except for number concentration.

the altitude, the model seems able to reproduce the trends for January and April. The accuracy of the July and October results is lower but remains satisfying, excluding the case of July, at 25 km. As the mixing ratio is a function of particle number density and also of air density, the steep increase at this altitude doesn't necessarily mean that more particles are formed at higher altitudes. Our calculations indicate that fewer particles are formed at higher altitudes (as expected from larger temperatures and lower sulphuric acid concentrations) but the decrease in the air density leads to an increase of the particle mixing ratio. For January and April, the model is able to broadly reproduce the change in aerosol mixing ratio with altitude, as observed by Hofmann and Rosen (1981) and predicted from Toon et al. (1979) using the Turco et al. (1979) model. In figure 11 we plot the predicted size ratio (N15/N25) as a function of altitude. It is clear that modelled values of size ratio match well with observed values taken from Hofmann and Rosen (1981) except for the case of April at 25 km. The main differences between our calculations and Timmreck and Graf's model (2000) probably lie in the method used to determine the gaseous sulphuric acid concentration. We used a profile determined from Toon et al. (1979), as Timmreck and Graf (2000) used a 3D model output to determine the main initial mixing ratios (water vapour, sulphur dioxide), and also calculated a rate of transformation of SO_2 into H_2SO_4. As nucleation schemes are sensitive to the initial amount of sulphuric acid (e.g. Vehkamäki et al., 2002), large differences could come from different H_2SO_4 initialisations. Moreover, discrepancies between our results and measurements may come from the fact we used zonally averaged temperature from ECMWF to get the atmospheric conditions, and not exactly the experimental ones, in Laramie. Finally, figure 12 illustrates the behaviour of the mixing and the size ratio (MR and SR respectively) as a function of the gas phase sulphuric acid concentration. When the initial amount of acid is high, both nucleation and the subsequent growth of

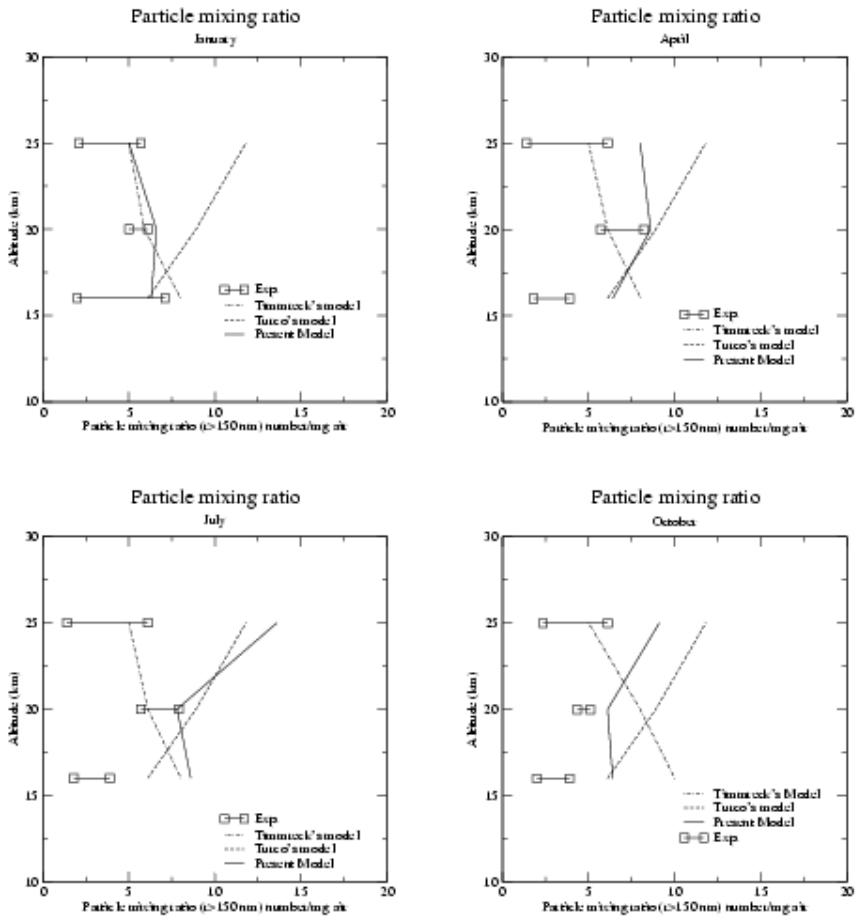

Figure 10: Top left panel: Numerical values of particle mixing ratio (MR), ($N(r > 0.15\ \mu\text{m})$), as a function of altitude for January conditions. Also shown are observed values taken from the measurements of Hofmann and Rosen (1981) and modelled values from Toon et al. (1979) and Timmreck and Graf (2000). The same results are presented for April (top right), July (bottom left) and October (bottom right) conditions.

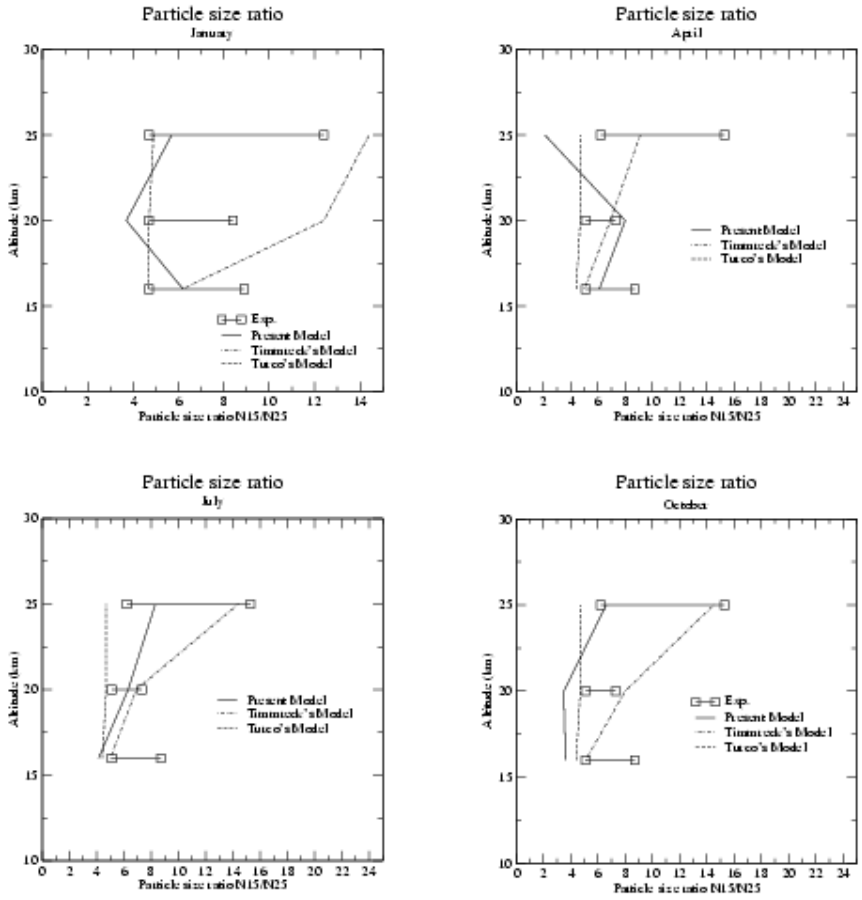

Figure 11: Top left panel: Numerical values of particle size ratio (SR), ($N(r > 0.15\ \mu\text{m})/N(r > 0.25\ \mu\text{m})$), as a function of altitude for January conditions. Also shown are observed values taken from the measurements of Hofmann and Rosen (1981) and modelled values from Toon et al. (1979) and Timmreck and Graf (2000). The same results are presented for April (top right), July (bottom left) and October (bottom right) conditions.

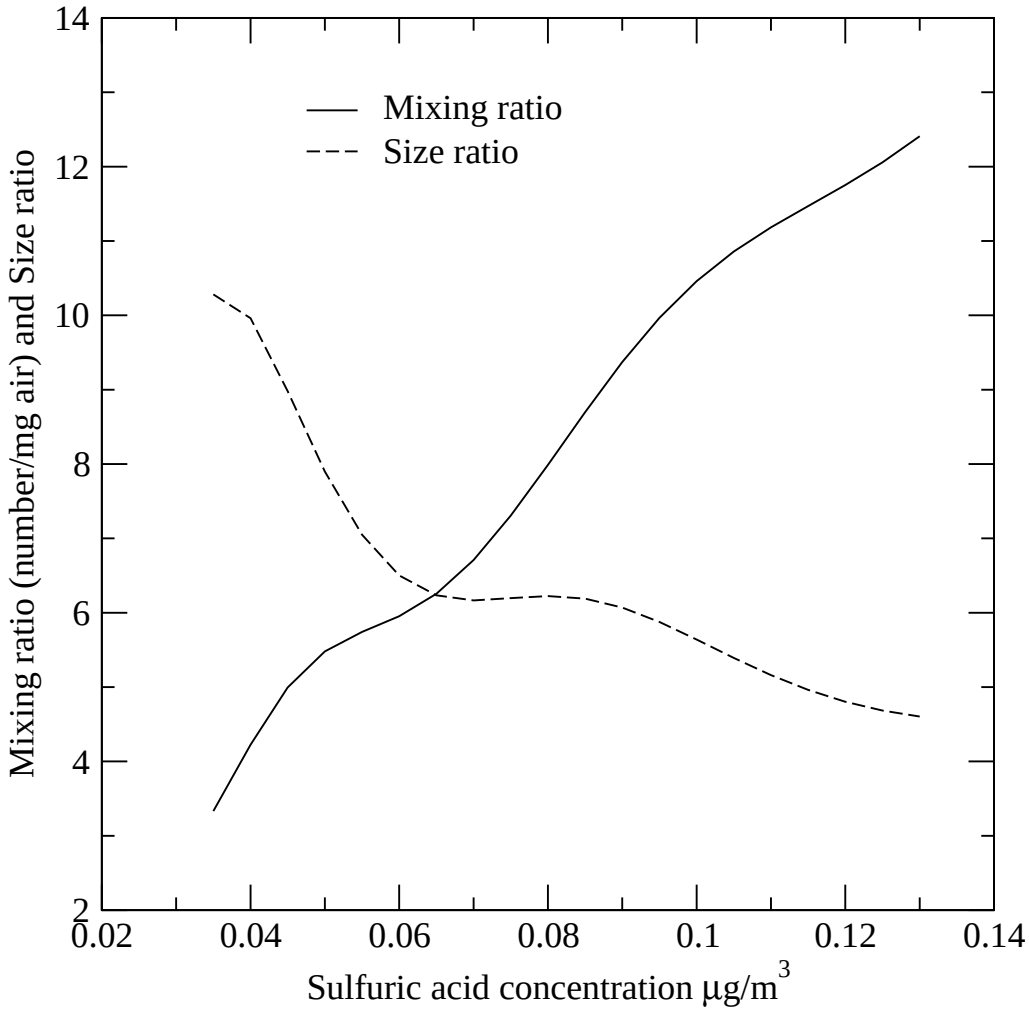

Figure 12: Evolution of the mixing and the size ratio of particles, as a function of the initial gas phase H_2SO_4 concentration, at 16 km.

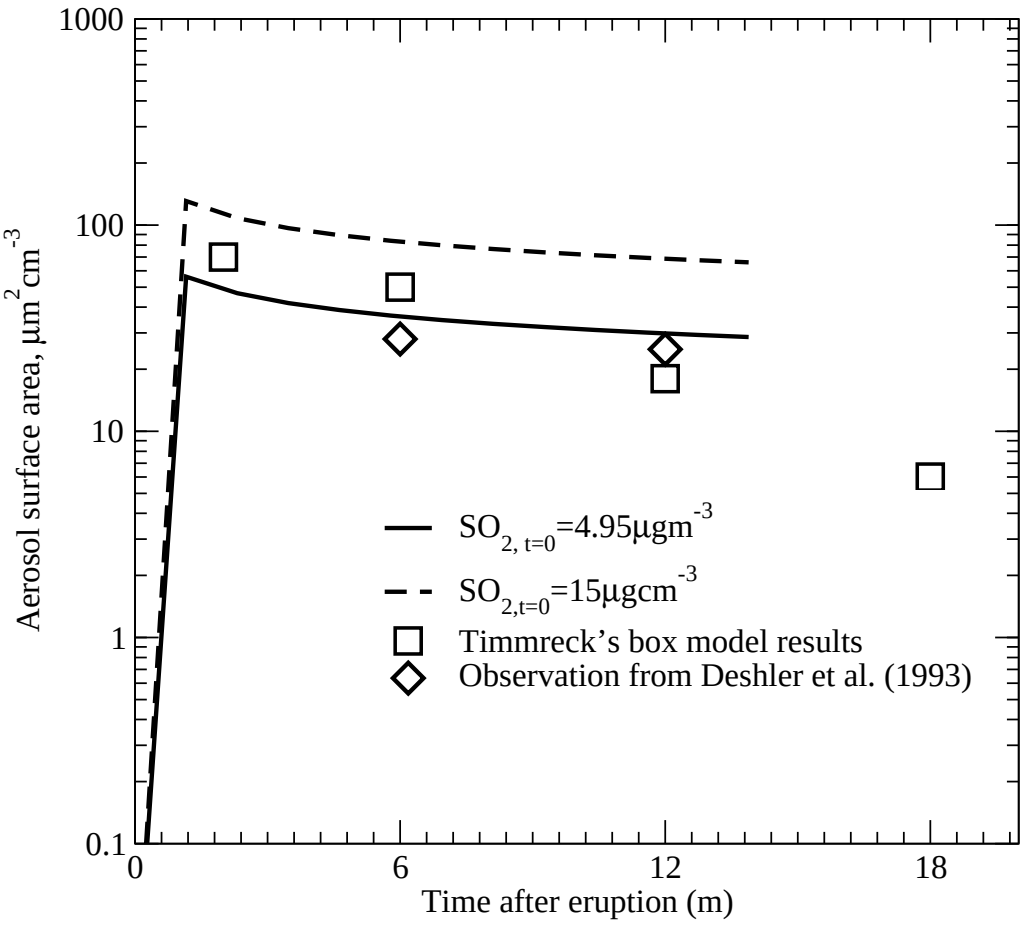

Figure 13: Evolution of the mixing and the size ratio of particles, as a function of the initial gas phase H_2SO_4 concentration, at 16 km.

particles are enhanced, producing high number concentrations of particles larger than 0.15 μm (N15). The solid line plot shows this trend for an altitude of 16 km. As more sulphuric acid is available, N25 increases faster than N15, leading to a total decrease of the size ratio (SR), as plotted by the dashed line and as expected.

5 Simulation of Mt. Pinatubo Volcanic Aerosols

After major volcanic eruptions, large amounts of water vapour, SO_2 and ash particles are injected into the atmosphere.

An enhanced SO_2 concentration has a major impact on the stratospheric background aerosol. Changes in H_2O and OH concentration can also influence the aerosol size distribution. Nevertheless, there is no agreement as to the amount of water vapour reaching the stratosphere. Therefore, changes in H_2O concentrations are neglected when simulating volcanic eruptions. The initial aerosol size distribution is assumed to be log-normal for a total number concentration N_0 = 10^7 m^{-3}, a standard deviation s = 1.8 and a mean radius r_m 7.10^{-8} m. Typical stratospheric atmospheric aerosol distributions can be represented by:

$$N_i = \frac{N_0}{r_i \ln s\sqrt{2\pi}} \exp\left(-0.5\left(\frac{\ln(r_i/r_m)}{\ln s}\right)^2\right). \quad (37)$$

A comparison between the calculated evolution of aerosol surface area and measurements by Deshler et al. (1993) at 20 km height is given in figure 13. We see that, for initial SO_2 concentrations of 4.95 μg m^{-3}, simulated aerosol surface is a reasonable match compared to the observed values. However, for larger initial concentrations of SO_2 the model fails to reproduce the observed development of aerosol surface area.

6 Conclusions

A fast aerosol microphysical model for the stratosphere has been developed. It simulates homogeneous nucleation of sulphuric acid-water aerosols, condensational growth, coagulation among particles and sedimentation. The model uses a non-iterative scheme to solve final number concentration of particles undergoing these processes. It is computationally fast: this makes the model ideal for importing into 3D global models. The present model has been used to simulate background stratospheric aerosol size distribution. The modelled size distribution parameters match well within the range of observed and earlier reported values. Two types of sensitivity studies are performed to see the effects of (a) changes in number of size bins and time step and (b) changes in environmental input parameters on aerosol size distribution. We find that the model is sensitive to the choice of number of size bins used. However, change in background aerosol surface area is not significant between high and low time and size resolved experiments. The modelled size distribution is found to be most sensitive to sulphuric acid gaseous concentration. A simplified case of Pinatubo volcanic eruption is used to simulate the aerosol temporal development. These first results are encouraging and will be followed by further development. The model that has been conceived, keeping in mind the need for computing efficiency, will soon be included in SLIMCAT, and will provide a powerful tool for aircraft emissions global impact studies.

Notation

a	Offset for σ linear dependence on temperature.
A	Avogadro number.
b	Slope for σ linear dependence on temperature.
$c_{i,t}$	Mole concentration of H_2SO_4 in a particle from bin i at time t, in mole m^{-3}.
C_t	Mole concentration of gaseous H_2SO_4 in the atmosphere at time t in mole m^{-3}.
$C_{i,t}^{sat}$	Mole concentration of saturated H_2SO_4 vapour in the atmosphere at time t, above a particle from bin i, in mole m^{-3}.
Cc	Cunningham slip factor.
δ_i	Mean inter-particle distance (centre to surface), for bin i, in m.
d	Diameter of a molecule of H_2SO_4 in m.
D_i, D_i^p	H_2SO_4 and particle diffusion coefficient, in m^2 s^{-1}.
f_i	Volume fraction of H_2SO_4 in a critical cluster placed in bin i.
F_i	Ventilation factor for a particle in bin i.
g	Gravitational constant in m s^{-2}.
γ_i	H_2SO_4 activity in a solution having the same composition as a droplet in bin i.
$k_{i,t}$	Mass transfer rate s^{-1} of gaseous H_2SO_4 onto a particle from bin i.
$k_{i,t}^{nuc}$, $k_{i,t}^{growth}$	Same as $k_{i,t}$ for nucleation and growth (for both simultaneously, the superscript tot is used).
k_B	Boltzmann constant in J K^{-1}.
$K_{i,j}$	Coagulation kernel for a collision between particles from bins i and j, in m^3 s^{-1}.
K	Prefactor similar to k.
Kn_i	Knudsen number for a particle in bin i.
λ, λ_a, λ_i^p	Respectively air, sulphuric acid and particle mean free path, in m.
η_a	Dynamic viscosity of air in kg m^{-1} s^{-1}.
m_a, $m_{H_2SO_4}$	Molecular weight of air and sulphuric acid respectively, in kg $mole^{-1}$.
n_i	Number of H_2SO_4 molecules contained in a particle from bin i.
N, $N_{i,t}$	Respectively particle number density and particle number density in bin i, at time t in m^{-3}.
N_0	Particle total number density, in m^{-3}.
p_{H_2O}	Water vapour pressure, in Pa.
$p_{H_2O}^{sat}$	Water saturation vapour pressure above a droplet, in Pa.
p	H_2SO_4 vapour pressure in Pa.
p^{sat}	H_2SO_4 saturation vapour pressure above a flat surface of pure H_2SO_4 in Pa.

ρ_{a}, $\rho_{\mathrm{H_2SO_4}}$, ρ_i	Density of air, pure sulphuric acid and particle in bin i respectively, in kg m^{-3}.
r_i	Radius of a particle in bin i, in m.
$\mathrm{r_m}$	Mean radius of the lognormal size distribution, in m.
R	Universal gas constant J mole^{-1} K^{-1}.
σ_i	Particle (bin i) surface tension in J m^{-2}.
s	Standard deviation for a lognormal distribution.
$\mathrm{S}_{i,t}$	Saturation ratio of H_2SO_4 above a particle (bin i, time t) composed of pure H_2SO_4.
$\theta_{i,j,k}$	Bin partitioning function.
t	Time in s.
T	Temperature in K.
v	Wind velocity in m s^{-1}.
$\mathrm{v}_i^{\mathrm{sed}}$	Sedimentation velocity of a particle, in m s^{-1}.
$\mathrm{v_a}$, $\mathrm{v_{H_2SO_4}}$, $\mathrm{v}_i^{\mathrm{p}}$	Thermal velocity respectively of air, sulphuric acid molecules and particles in m s^{-1}.
$V_{\mathrm{m},i}$	Volume of H_2SO_4 per mole in a solution having the same composition as a particle from bin i, in m^3 mole^{-1}.
V_i	Volume of a particle from bin i, in m^3.
W_i	Sulphuric acid weight fraction in a particle from bin i.

Acknowledgments

The authors acknowledge funding of this work by a NERC UTLS-Ozone Grant NER/T/S/2000/01032. The authors would also like to thank H. Vehkamäki for providing her nucleation model and for helpful discussions.

References

Ayers, G. P., R. W. Willet, and J. L. Gras, On the vapour pressure of sulphuric acid, *Geophys. Res. Lett., 7*, 433-436, 1980.

Bekki, S., and J. A. Pyle, Two-dimensional assessment of the impact of aircraft sulphur emissions on the stratospheric sulphate aerosol layer, *J. Geophys. Res., 97*, 15839-15847, 1992.

Bekki, S., and J. A. Pyle, A two-dimensional modelling study of the volcanic eruption of Mount Pinatubo, *J. Geophys. Res., 99*, 18861-18869, 1994.

Bigg, K. E., Stratospheric particles, *J. Atmos. Sci., 32*, 910-917, 1975.

Brock, C. A., P. Hamill, J. C. Wilson, H. H. Jonhson, and K. R. Chan, Particle formation in the upper tropical troposphere: A source of nuclei for the stratospheric aerosol, *Science, 270*, 1650-1653, 1995.

Brown, R. C., R. C. Miake-Lye, M. R. Anderson, C. E. Kolb, and T. J. Resch, Aerosol dynamics in near-field aircraft plumes, *J. Geophys. Res., 101*, 22939-22954, 1996.

Cadle, R. D., and C. S. Kiang, Stratospheric Aitken particles near the tropopause, *Rev. Geophys. Space Phys., 15*, 195-202, 1977.

Clegg, S. L., Application of a multi-component thermodynamic model to activities and thermal properties of 0-40 mol kg^{-1} aqueous sulphuric acid from < 200 to 328 K, *J. Chem. Eng. Data, 40*, 43-64, 1995.

Clegg, S. L., P. Brimblecombe, and A. S. Wexler, A Thermodynamic model of the system H^+-NH_4^+-SO_4^{2-}-NO_3^--H_2O at tropospheric temperatures, *J. Phys. Chem., 102A*, 2137-2154, 1998.

Clement, C. F., M. Kulamala, and T. Vesala, Theoretical considerations on sticking probabilities, *J. Aerosol Sci., 27*, 869-882, 1996.

Davies, E. J., Transport phenomena with single aerosol particles, *Aerosol Sci. Technol., 2*, 121-44, 1983.

Deshler, T., D. J. Hofmann, B. J. Johnson, and W. R. Rozier, Balloonborne measurements of the Pinatubo aerosol size distribution and volatility at Laramie, Wyoming during the summer of 1991, *Geophys. Res. Lett., 19*, 199-203, 1992.

Deshler, T., B. J. Johnson, and W. R. Rozier, Balloonborne measurements of the Pinatubo aerosol during 1991 and 1992 at 41°N: Vertical profiles, size distribution and volatility, *Geophys. Res. Lett., 20*, 1435-1438, 1993.

Friedlander, S. K., *Smoke, Dust and Haze. Fundamentals of Aerosol Dynamics*, Oxford University Press, New York, 2000.

Fuchs, N. A., *The Mechanics of Aerosols*, Pergamon Press, New York, 1964.

Fuchs, N. A., and A. G. Sutugin, Highly dispersed aerosols, *Topics in Current Aerosol Research, 2*, Pergamon Press, New York, 1-60, 1971.

Hofmann, D. J., S. J. Oltmans, J. M. Harris, S. Solomon, T. Deshler, and B. J. Johnson, Observation and possible causes of new ozone depletion in Antarctica in 1991, *Nature, 359*, 283-287, 1992.

Hofmann, D. J., and S. Solomon, Ozone destruction through heterogeneous chemistry following the eruptions of El Chichon, *J. Geophys. Res., 94*, 5029-5041, 1989.

Hofmann, D. J., and J. M. Rosen, On the background stratospheric aerosol layer, *J. Atmos. Sci., 32*, 1446-1456, 1981.

Hofmann, D. J., T. J. Pepin, and R. G. Pinnick, Stratospheric aerosol measurements. I: Time variations at northern midlatitudes, *J. Atmos. Sci., 32*, 1446-1456, 1975.

Jacobson, M. Z., Numerical techniques to solve condensational and dissolutional growth equations when growth is coupled to reversible reactions, *Aerosol Sci. Technol., 27*, 491-498, 1997.

Jacobson, M. Z., *Fundamentals of Atmospheric Modelling*, Cambridge University Press, Cambridge, UK, 1999.

Jacobson, M. Z., Analysis of aerosol interactions with numerical techniques for solving coagulation, nucleation, condensation, dissolution, and reversible chemistry among multiple size distributions, *J. Geophys. Res., 107*, doi:10.1029/2001JD002044, 2002.

Jacobson, M. Z., R. P. Turco, E. J. Jensen, and O. B. Toon, Modelling coagulation among particles of different composition and size, *Atmos. Environ., 28*, 1327-1328, 1994.

Jacobson, M.Z., and R. C. Turco, Simulating condensational growth, evaporation, and coagulation of aerosols using moving and stationary size grid, *Aerosol Sci. Technol., 22*, 73-92, 1995.

Kärcher, B., Physicochemistry of aircraft-generated liquid aerosols, soot, and ice particles, 1. Model description, *J. Geophys. Res., 103*, 17111-17128, 1998.

Kulmala, M., A. Laaksonen, Binary nucleation of water-sulphuric acid system: Comparison of classical theories with different H_2SO_4 saturation vapor pressures, *J. Chem. Phys., 93*, 696-701, 1990.

Kulmala, M., A. Laaksonen, and L. Pijrola, Parameterisation for sulphuric acid/water nucleation rates, *J. Geophys. Res., 103*, 8301-8308, 1998.
Lacis, A., J. Hansen, and M. Sato, Climate forcing by stratospheric aerosols, *Geophys. Res. Lett., 19*, 1607-1610, 1992.
List, R. J. ed., Smithsonian Meteorological Tables, 6th ed., Smithsonian Institution Press, Washington DC, 1984.
Michaelangeli, D., M. Allen, Y. L. Yung, R. L. Shia, D. Crisp, and J. Eluszkiewicz, Enhancement of atmospheric radiation by an aerosol layer, *J. Geophys. Res., 97*, 865-974, 1992.
Nair, P. V. N., and K. G. Vohra, Growth of aqueous sulphuric acid droplets as a function of relative humidity, *J. Atmos. Sci., 6*, 265, 1975.
Noppel, M., H. Vehkamäki, and M. Kulamala, An improved model for hydrate formation in sulphuric acid-water nucleation, *J. Chem. Phys., 116*, 218-228, 2002.
Pitari, G., V. Rizi, L. Ricciardulli, and G. Visconti, High-speed civil transport impact: Role of sulphate, nitric acid trihydrate, and ice aerosols studied with a two-dimensional model including aerosol physics, *J. Geophys. Res., 98*, 23141-23164, 1993.
Pruppacher, H. R. and J. D. Klett, *Microphysics of Clouds and Precipitation*, Kluwer Academic Publishers, Dordrecht, 1997.
Reiss H., The kinetics of phase transitions in binary systems, *J. Chem. Phys., 18*, 840-848, 1950.
Rodriguez, J. M., M. K. W. Ko, and N. D. Sze, Role of heterogeneous conversion of N_2O_5 on sulphate aerosols in global ozone losses, *Nature, 352*, 134-137, 1991.
Rosen, J. M., D. J. Hofmann, and J. Laby, Stratospheric aerosol measurements. The worldwide distribution, *J. Atmos. Sci., 32*, 1457-1462, 1975.
Solomon S., R. R. Garcia, F. S. Rowland, and D. J. Wuebbles, On the depletion of Antarctic ozone, *Nature, 321*, 755, 1986.
Sorokin A., X. Vancassel, and P. Mirabel, On volatile particle formation in aircraft exhaust plumes, *Phys. Chem. Earth (C), 26*, 557-561, 2001.
Steele, H. M., and P. Hamill, Effects of temperature and humidity on the growth and optical properties of sulphuric acid-water droplets in the stratosphere, *J. Aerosol Sci., 12*, 517-528, 1981.
Tie, X., L. Lin, and G. Brasseur, Two-dimensional coupled dynamical/chemical/microphysical simulations of global distribution of El Chichon volcanic aerosols, *J. Geophys. Res., 99*, 16779-16792, 1994.
Timmreck, C., and H. F. Graf, A microphysical model for simulation of stratospheric aerosol in a climate model, *Meteorolog. Zeit., 9*, 263-282, 2000.
Timmreck, C, Three-dimensional simulations of stratospheric background aerosol: First results of a multiannual GCM simulation, *J. Geophys. Res., 106*, 28313-28332, 2001.
Toon, O. B., R. P. Turco, P. Hamill, C. S. Kiang, and R. C. Whitten, A one-dimensional model describing aerosol formation and evolution in the stratosphere: II. Sensitivity studies and comparison with observations, *J. Atmos. Sci., 36*, 718-736, 1979.
Toon, O. B., R. P. Turco, D. Westphal, R. Malone, and M. S. Liu, A multidimensional model for aerosols: Description of computational analogs, *J. Atmos. Sci., 45*, 2123-2143, 1988.
Turco, R. P., P. Hamill, O. B. Toon, R. C. Whitten, and C. S. Kiang, A one-dimensional model describing aerosol formation and evolution in the stratosphere, I. Physical processes and mathematical analogs, *J. Atmos. Sci., 36*, 699-717, 1979.
Van Dingenen, R., and F. Raes, Determination of the condensation accomodation coefficient of sulphuric acid on water-sulphuric acid aerosol, *Aerosol Sci. Tech., 15*, 93-106, 1991.

Vehkamäki, H., M. Kulmala, I. Napari, K. E. J. Lehtinen, C. Timmreck, M. Noppel, and A. Laaksonen, An improved parameterisation for sulphuric acid/water nucleation rates for tropospheric and stratospheric conditions, *J. Geophys. Res., 107*, doi: 10.1029/2002JD002184, 2002.

Weisenstein, D. K., P. K. Yue, G. K. W. Ko, N. D. Sze, J. M. Rodriguez, and C. J. Scott, Two-dimensional model of sulphur species and aerosol, *J. Geophys. Res., 102*, 13019-13053, 1997.

Yu, F., and R. P. Turco, The role of ions in the formation and evolution of particles in aircraft plumes, *Geophys. Res. Lett., 24*, 1927-1930, 1997.

Yue, G. K., The formation and growth of sulfate aerosols in the stratosphere, *Atmos. Environ., 15*, 549-556, 1981.

Yue, G. K., and A. Deepak, Temperature dependence of the formation of sulphate aerosols in the stratosphere, *J. Geophys. Res., 87*, 3128-3134, 1982.

Zeleznik, F. J., Thermodynamic properties of the aqueous sulphuric acid system to 350 K, *J. Phys. Chem. Ref. Data, 20*, 1157-1200, 1991.

Zhao, J. X., R. P. Turco, and O. B. Toon, A model simulation of Pinatubo volcanic aerosols in the stratosphere, *J. Geophys. Res., 100*, 7315-7328, 1995.